



Search for Excess Dimuon Production in the Radial Region $1.6 < r \lesssim 10$ cm at the DØ Experiment

The DØ Collaboration
URL: <http://www-d0.fnal.gov>
(Dated: March 29, 2009)

We report on a study of events containing at least two muons produced in $p\bar{p}$ collisions at $\sqrt{s} = 1.96$ TeV, performed at the DØ experiment using data corresponding to 0.9 fb^{-1} of integrated luminosity collected during 2008. Motivated by a recent claim of an excess in muons produced at large radius by the CDF collaboration [1], we study muons that appear to be produced with a radius between 1.6 and 10 cm from the initial $p\bar{p}$ collision point. The experimental signature is a well reconstructed muon that is missing hits in the innermost layer of the tracking detector. We record 28 374 muons that appear to be produced without hits in the first layer of the tracking detector. Based on the measured hit inefficiency, we expect $27\,662 \pm 503 \pm 1027$ muons from the primary interaction to not have a reconstructed hit in this layer. This gives an observed excess of $712 \pm 462 \pm 942$ events in which one or both muons are produced in the range $1.6 < r \lesssim 10$ cm, which is expressed as a fraction $(0.40 \pm 0.26 \pm 0.53)\%$ of the total dimuon sample. A small level of excess is expected due to cosmic rays, decays-in-flight of pions and kaons, and hadronic punchthrough, and first estimates of these contributions are made. We therefore see no anomalously large excess of muons produced a few centimeters away from the interaction point.

Preliminary Results for Winter 2009 Conferences

1. INTRODUCTION

The primary source of dimuon events at the Tevatron collider at Fermilab is the production and subsequent decay of heavy quark-antiquark pairs, $b\bar{b}$ and $c\bar{c}$ [2, 3], as well as the direct decay of $b\bar{b}$ and $c\bar{c}$ resonances, such as J/ψ and Υ mesons. Measurements of the $b\bar{b}$ production cross-sections using semileptonic decays are sensitive to the muon production rate. A history of discrepancies in these cross-sections between experimental results and theoretical expectations has prompted further investigation from both sides, leading to improved convergence between theory and experiment in recent years [4].

The CDF collaboration has recently presented a study indicating a significant sample of dimuon events in which one or both muons appear to be produced at large radial distances (> 1.5 cm) from the primary interaction point [1]. The findings are inconsistent with current heavy quark production models, with the excess having a magnitude comparable to the contribution from $b\bar{b}$ production. Analysis of these so-called “ghost” muons shows that they have characteristic long tails in their impact parameter (IP) distribution^[a], relative to the corresponding distribution for heavy flavor events. However, the vast majority of ghost muons have impact parameters of 1 cm or less. The study also indicates the presence of large numbers of additional muons in the angular vicinity of the ghost muons, inconsistent with sequential semileptonic decays of b hadrons.

In this note, we describe a corresponding search at D0 for dimuon events in which one or both muons are produced at radial distances exceeding 1.6 cm, relative to the primary $p\bar{p}$ interaction. The upper limit on this radial acceptance ($r \lesssim 10$ cm) is set by additional hit requirements in the D0 silicon vertex detector. The search is performed using information from the innermost layer of the silicon detector. Once the sample of such events has been determined, some of their properties are investigated by comparing the distributions of various parameters with the expectations. The D0 detector differs in important respects from the CDF detector and thus offers a useful cross-check of the ghost muon study. Compared with CDF, D0 has a smaller decay volume and has more interaction lengths of material before the muon identification.

2. THE D0 DETECTOR

D0 is a general purpose colliding beam detector described in detail elsewhere [5]. The most important detector components for this analysis are the tracking and muon systems in the central region corresponding to pseudorapidity^[b] $|\eta| < 1.0$. In the following description, a cylindrical coordinate system (r, ϕ, z) is used, with the z -axis along the proton beam direction; the radial and azimuthal coordinates are defined in the usual way, such that an angle of $\phi = \pi/2$ ($3\pi/2$) corresponds to an upward (downward) direction. For certain vector quantities (such as momentum), a transverse component is defined by the projection onto the (r, ϕ) plane. The effective interaction region of $p\bar{p}$ bunch crossings is approximately Gaussian in z , with mean $\mu_z = 0$ and standard deviation $\sigma_z \approx 25$ cm; the transverse extent of the beam is typically $25 \mu\text{m}$ [5].

The central tracking detector at D0 is contained within a 2 T solenoidal field, and formed from two different subsystems, the silicon microstrip tracker (SMT) and the central fiber tracker (CFT). The silicon tracker consists of six barrel/disk modules, two outer disks, and an inner layer (layer-zero, or L0). The barrels each have 8 staggered half-layers of sensors to achieve 4 layers of complete coverage between radii of 2.7 and 10.0 cm. All barrel sensors in the central region are instrumented with two detection surfaces, “axial” and “stereo”, to improve the single hit resolution. Each barrel is 12 cm long and is capped by a disk with an inner radius of 2.7 cm and outer radius of 10.5 cm. The L0 detector [6] surrounds the beryllium beampipe, and consists of single-sided sensors staggered at radii of 1.60 and 1.76 cm to provide 98% ϕ coverage, in the range $|z| < 38$ cm. The central silicon detector is therefore instrumented with four double-sided and one single-sided layer of concentric silicon sensors for incident particles with $|\eta| < 1.0$. For the time period considered during this analysis, one of the sensors in L0 was inactive; this must be taken into account during event selection, as described later. The CFT consists of 16 concentric layers of scintillating fiber surrounding the beampipe, at radial distances of 20 cm to 50 cm. Information from both tracking systems is combined for use in triggering and track reconstruction. The geometrical alignment of the SMT system is known to within $7 \mu\text{m}$ in the transverse plane, and $15 \mu\text{m}$ in z ; the CFT alignment is known to within $20 \mu\text{m}$.

The muon system in the $|\eta| < 1$ region is constructed in three layers, A, B, C, and consists of a combination of proportional drift tubes (PDTs) and scintillation counters [7]. The innermost layer (A) is formed from three or four sub-layers of PDTs capped by one sub-layer of scintillation counters, and surrounds the calorimeter, which is 5.5–7.4

[a] The impact parameter of a track is its extrapolated distance-of-closest-approach to the primary $p\bar{p}$ interaction, in the (r, ϕ) plane.

[b] The pseudorapidity η of a track is defined by $-\ln[\tan(\theta/2)]$, where θ is the polar angle with respect to the proton beam direction.

interaction lengths, λ , in depth. Surrounding layer A is an iron toroid of thickness 1.09 m, providing a magnetic field of 1.8 T to aid in muon identification and reconstruction. Layer B is mounted on the outside of the toroid, and consists of three sub-layers of PDTs. The outermost layer (C) is separated from layer B by ~ 1 m, and formed from three sub-layers of drift tubes and an additional sub-layer of scintillation counters. This three-layer coverage extends over the upper three sides of the central muon system, with much of the underside of the detector only covered by two layers due to obstruction by structural detector supports. Scintillation counters are mounted on the B layer for part of this region. The total thickness traversed by muons exiting the iron is 12.8–14.5 λ giving a minimum momentum of around 3 GeV/ c for that muon topology. The scintillation counters have time resolutions of ~ 3 ns.

3. TRIGGERS

The fast-readout capabilities of the muon scintillation counters and drift chambers allow muons to be identified at all three levels of the D0 trigger system. In this analysis, no particular trigger requirements are enforced (i.e. events are accepted from all triggers, inclusively), in order to maximise the opportunity to observe different types of events. However, as a cross-check of the possible biasing effects of the triggers, the procedure to count the number of excess dimuon events is repeated using only those events which satisfy a dedicated dimuon trigger.

This trigger requires two muons with $p_T > 2.0$ GeV/ c to be present in the region $|\eta| < 2.0$, and to pass predefined hit requirements in the muon scintillators and drift chambers. The time of detection for at least one of the muons must be consistent with the bunch crossing time (within ± 10 ns), and a primary vertex must be found within $|z| < 35$ cm. The muons are not required to be matched with a central track. These requirements are significantly looser than those applied during the offline dimuon selection. Note that the ± 10 ns scintillator timing requirement is very efficient ($> 99\%$) for beam-produced muons, but no attempt is made to determine the efficiency for long-lived massive charged particle candidates.

Examination of the $J/\psi \rightarrow \mu^+\mu^-$ test sample (see Section 6) and the signal dimuon sample (Section 5) indicates that this dimuon trigger is satisfied for more than half of all selected dimuon events. For the J/ψ sample, this fraction is 62%; for the signal dimuon sample, the fraction is 70%. The remainder of events typically trigger on other single or dimuon triggers which include a track-matching requirement. The D0 trigger system is thus expected to be sensitive to muons originating outside the beampipe, with the impact parameter aperture larger than the corresponding limit applied during offline reconstruction.

4. RECONSTRUCTION

a. Track and Vertex Finding

Particle track candidates are identified from hits in the SMT and CFT detectors using a combination of different pattern recognition algorithms, and the resulting global set of track candidates are refitted with an improved calculation of track parameters, using a full Kalman fit road-finding technique. The refit takes into account the details of the magnetic field and the detector material, including multiple scattering and energy losses. This analysis uses the standard D0 track reconstruction software. The following text describes the track-finding algorithm which is most efficient for particles with impact parameters larger than a few millimeters.

The starting point for a track candidate is a track seed constructed from three consistent SMT clusters, which must have curvature corresponding to $p_T > 450$ MeV/ c and an impact parameter smaller than 2.5 cm. This seed is then extrapolated outward through the SMT and CFT systems, constructing track hypotheses by iteratively associating any additional hits that are consistent with the seed. The extrapolation continues to the outermost CFT layer, or until three consecutive misses are allocated to the end of a track; additional track quality criteria are then imposed based on the arrangement of hits and misses for each hypothesis.

To allow tracks with fewer than three SMT hits to be reconstructed, the procedure is repeated starting from CFT-only track seeds, also using three clusters. In this case the combinatorics are reduced significantly by using the SMT-seeded tracks in the same event to measure the location of the $p\bar{p}$ interaction(s). The CFT seeds are then required to pass within 1.5 cm, in z and in transverse distance, of one of these interaction points. The CFT seeds are also extrapolated back into the SMT system to associate any consistent silicon hits with the track. The tracks which are sent to the global tracking refit therefore have three or more hits in either the SMT or CFT sub-detectors, and are constrained to have impact parameter less than 2.5 cm (1.5 cm) in the SMT (CFT) case.

Following track reconstruction, the positions of primary vertices (PV) in each event are determined from a set of selected tracks, filtered to remove long-lived particles, or those which may have interacted with the detector material, using the method described in Ref. [8]. These are fitted to vertices using a χ^2 minimization procedure, yielding PV

positions to a precision of $35 \mu\text{m}$ along the beam direction [5]. The track impact parameter is calculated at the z -coordinate of the primary vertex, and typically has an uncertainty of $15 \mu\text{m}$ for $p_T > 3 \text{ GeV}/c$ tracks.

D0 has previously searched for neutral, long-lived particles decaying to two muons [9, 10]. That analysis used a different data sample and required the muons to be isolated and have $p_T > 10 \text{ GeV}/c$. Studies undertaken for that analysis measured the reconstruction efficiency, using simulated decays of K_S mesons, as a function of the radial displacement between the primary interaction and the decay vertex. The results show that this efficiency is unchanged up to vertex displacements of $\sim 15 \text{ cm}$, falling to around half its maximum level by 25 cm . It is therefore expected that the D0 reconstruction software has the required acceptance and efficiency to observe muons arising from secondary vertices at radii $\lesssim 25 \text{ cm}$, provided that their impact parameters are less than $\sim 2.5 \text{ cm}$.

b. Muon Reconstruction

Muons are first reconstructed by associating hits in the muon drift chambers into short tracks called segments, with timing and position information from the scintillation counters used to further constrain the muon trajectories. In this analysis, muons are only accepted if they have segments in both the A-layer and the combined BC-layer. In addition, muons are required to be associated with hits in both the A and C layer scintillators, to aid removal of cosmic ray muons and other backgrounds by appropriate use of timing information.

Segments from layers B and C are first combined, provided that they match in position and angle. The BC segments are then passed to the next stage, for matching to A segments. Angular and position variables are used to test compatibility of A-BC segments, with the curvature resulting from the intermediate toroid magnet taken into account. Each BC segment can be matched to multiple A segments, provided that they satisfy these compatibility tests. The resulting muon candidates are refitted using hits from all three layers to produce “local” muon objects.

Reconstructed local muons are matched to charged particle tracks in the central tracking detector by extrapolating inward from the muon track. If multiple tracks are found which match a local muon, the candidate with the lowest total χ^2 is selected. The combined track parameters and uncertainties are then taken from the central track. For isolated local muons, track matching is performed with an efficiency of $> 95 \%$, determined using $Z \rightarrow \mu\mu$ data.

5. EVENT SELECTION

The analysis presented here uses data collected by the D0 experiment between August and December 2008, corresponding to a total integrated luminosity of around 0.9 fb^{-1} . The event selection scheme is designed to collect a dimuon sample to approximately match the kinematic requirements of the dimuon sample used by CDF in their analysis [1].

a. Selecting Dimuon Candidates

The dimuon sample is produced by selecting the two highest- p_T muons in each event, provided that they satisfy the following requirements. Both muons must fulfill standard D0 quality criteria, be associated with hits in both A- and combined BC-layers, and satisfy $p_T > 3 \text{ GeV}/c$ and $|\eta| < 1.0$. Both muons must be matched to central tracks. To prevent two muons produced in separate $p\bar{p}$ interactions in the same beam crossing from being associated into a dimuon candidate, the difference in their z -coordinates at the point-of-closest approach to the primary vertex [$\Delta z_0 = z_0(\mu_1) - z_0(\mu_2)$] must be less than 1.5 cm . In addition, the combined invariant mass of the dimuon pair, $M(\mu\mu)$, must lie in the range $5 < M(\mu\mu) < 80 \text{ GeV}/c^2$, to replicate the CDF selection. The exclusion of low-mass dimuons reduces the contribution from resonances (such as the J/ψ), cascade decays of single b quarks, and gluon splittings $g \rightarrow b\bar{b}$, where both b quarks have a lepton in their decay chain; the upper limit reduces the contribution from Z decays.

Contributions from cosmic ray muons are reduced using two independent criteria. Single cosmic ray muons that do not interact in the detector may be reconstructed as two opposite-sign muon candidates traveling back-to-back in the detector. For this case, a simple angular veto is imposed, removing opposite-sign muons that satisfy $\Delta\phi > 3.135$ radians, where $\Delta\phi$ is the azimuthal angular separation of the two particles at their point of closest approach to the PV.

However, this selection will not remove all cosmic ray muon contamination. It is possible that only one of the two muon legs associated with the cosmic track is reconstructed. These cases are even more common for so-called cosmic showers [11, 12], consisting of multiple muons traveling close together. In consideration of these additional sources of cosmic ray muons, the timing information from the muon scintillators is used to further reduce backgrounds of

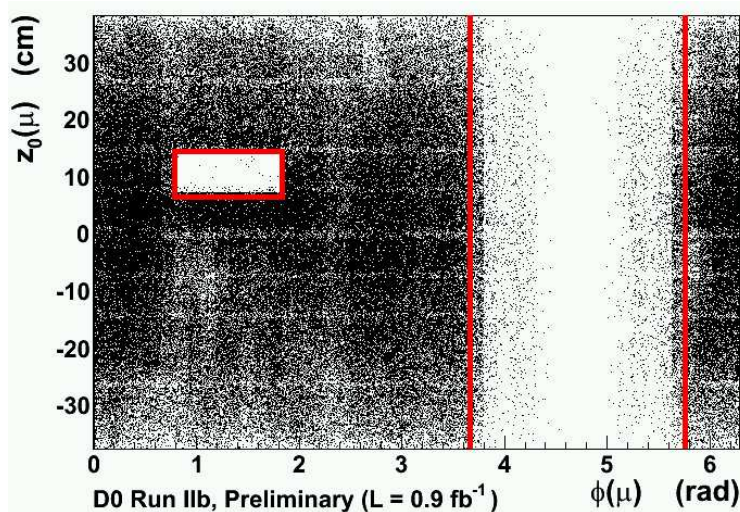


FIG. 1: Scatter plot of the (z, ϕ) coordinate of muons from $J/\psi \rightarrow \mu\mu$ decays, as they pass through layer zero (L0) of the silicon tracking detector. The unresponsive L0 element can be seen as a low-population box, while the limits on the acceptance of the muon system can be seen at $\phi \approx 4$ – 5.5 rad. Dimuon events are excluded if either muon lies within the regions highlighted.

this type. All muons must be associated with “in-time” scintillator hits in both layer A and layer C of the muon system. Here, in-time translates to detection within ± 10 ns of the expected muon arrival time, taking into account the bunch-crossing timing and the muon travel time from the primary vertex to the scintillator element. Since the detection time at the scintillators is offset to give an expected arrival time for beam-produced muons of 0 ns for both layer A and C, the pass criterion for each muon is defined by $|t(A)| < 10$ ns and $|t(C)| < 10$ ns.

For the purposes of this analysis, it is important that the muons are located in the central z -region of the detector, corresponding to the active range of the innermost layer (layer zero, i.e. L0) of the silicon detector. L0 has coverage $|z| < 38$ cm, so muons are excluded from the selection if their z -coordinate at L0, $z_{L0}(\mu)$, lies beyond these geometrical limits. For clarity, the resulting sample of dimuon candidates is hereafter referred to as the signal sample, to distinguish from a “test” selection described later in this note.

Finally, the single inactive sensor in L0 must be accounted for, by removing all events in which either muon crosses the detector in the (z, ϕ) range corresponding to this component. This can be seen in the (z, ϕ) scatter plot in Fig. 1, which shows the distribution of muons (from an independent sample of $J/\psi \rightarrow \mu^+\mu^-$ decays) which have hits in L0. Events are excluded from the selection if either muon lies in the range $3\pi/12 < \phi_{L0} < 7\pi/12$ radians, $6 < z_{L0} < 14$ cm, as shown by the superimposed box. Due to reduced A, B, C layer muon chamber coverage at the bottom of the detector, muons in the range of $14\pi/12 < \phi_{L0} < 22\pi/12$ are also excluded from the sample in the region of poor reconstruction efficiency as shown in Fig. 1.

b. Muons Produced within L0

The signal sample of dimuon candidates defined above has no requirements placed on the number of associated hits in the silicon detector. Since this analysis aims to study muon production in terms of radial distance from the primary vertex, two subsets of this sample are defined. The “loose” sample is defined by requiring that both muons in the event have three or more hits in the silicon tracker. The “tight” sample is a sub-set of the loose events, in which both muons have hits in L0 of the silicon detector. Events which are loose but not tight therefore contain at least one muon without a L0 hit, either due to hit inefficiencies, or production beyond L0. The radial acceptance of this selection is demonstrated in Fig. 2, which shows the (r, ϕ) arrangement of SMT sensors, and the associated distribution of the radius of the innermost hit on muon tracks that pass the loose selection. Muons are accepted even if produced at radial displacements of 10 cm from the z -axis, since the three-hit requirement can be satisfied by separate hits in the axial and stereo surfaces of a single sensor, along with an additional barrel or disk hit. For comparison, the CDF analysis [1] demands hits in three out of seven layers of their silicon detector tracker, hence accepting muons produced at radii up to ~ 10 cm.

If all muons were produced within L0, then the ratio of tight to loose events, $N(\text{tight})/N(\text{loose})$, would be given by the dimuon detection efficiency of L0 relative to the loose selection efficiency, $\varepsilon_{T/L}$. Conversely, the number of events

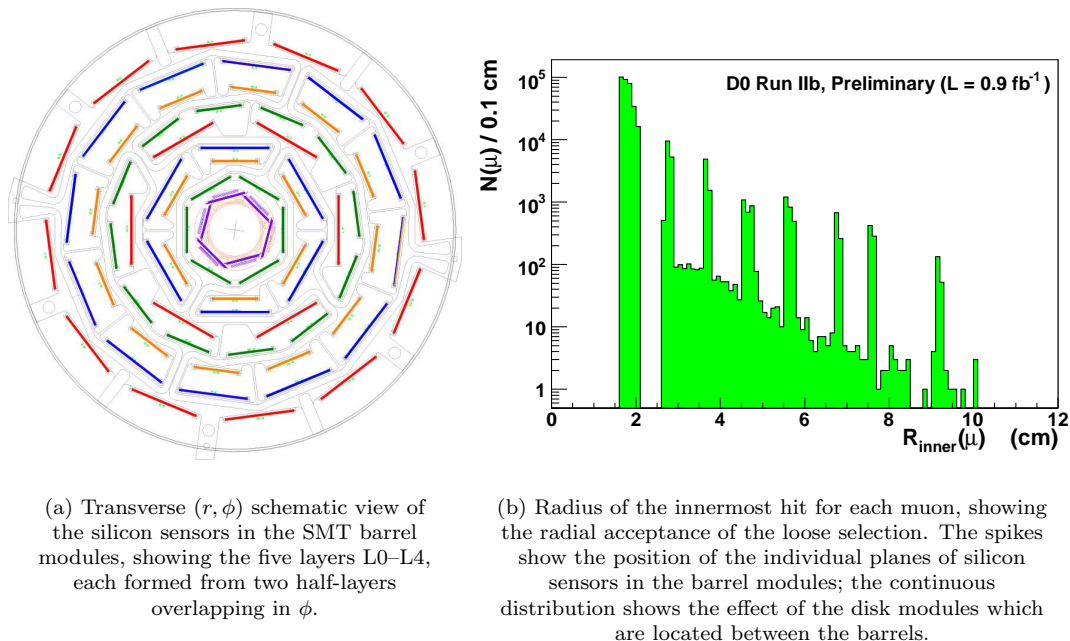


FIG. 2: Radial acceptance of the loose SMT requirement, showing the location of the barrel sensors in the transverse plane, and the resulting radial range in which muons can be accepted. The influence of the SMT design shown in (a) can clearly be seen by the peaks in (b). Muons are accepted even if produced at radial distances of 10 cm from the z -axis, with the number of hits falling approximately exponentially as is expected from individual hit efficiencies of $\sim 90\%$ per sensor.

containing one or both muons produced beyond L0, $N(\text{excess})$, can be measured by event counting:

$$N(\text{excess}) = N(\text{loose}) - \frac{N(\text{tight})}{\varepsilon_{T/L}}. \quad (1)$$

Since the muon detection efficiency may depend on a number of variables, such as p_T , ϕ , z or η , the efficiency $\varepsilon_{T/L}$ must be determined as a function of these variables. The subsequent counting procedure is then performed on an event-by-event basis, taking into account the properties of both muons in each event. The following section describes the method for extracting the efficiencies and measuring dependencies on various kinematic and geometrical variables.

6. MUON DETECTION EFFICIENCIES

a. The $J/\psi \rightarrow \mu^+ \mu^-$ Test Sample

To measure the relative efficiency of the tight and loose selection requirements, a test sample of $J/\psi \rightarrow \mu^+ \mu^-$ candidates is selected, and the number of tight and loose events is determined as a function of various muon variables. The sample is taken from the same 0.9 fb^{-1} data sample used for the signal dimuon selection described above. J/ψ candidates are selected from opposite-charge muons originating at a common vertex, and with invariant mass $2.95 < M(\mu\mu) < 3.2 \text{ GeV}/c^2$. This latter requirement ensures that there is no overlap between the J/ψ test sample and the signal dimuon sample, which requires a minimum dimuon invariant mass of $5 \text{ GeV}/c^2$.

To ensure matching between the kinematics of the test and signal samples, the muons from $J/\psi \rightarrow \mu^+ \mu^-$ decay must satisfy $p_T > 3 \text{ GeV}/c$, $|\eta| < 1.0$, and $|z_{L0}| < 38 \text{ cm}$, and also fulfill the same muon quality requirements. In addition, they must also pass the cosmic-reducing cuts $\Delta\phi < 3.135 \text{ rad}$, $|t(A)| < 10 \text{ ns}$ and $|t(C)| < 10 \text{ ns}$. Finally, events with either muon in the inactive (z, ϕ) regions are excluded with the same cut as applied to the signal sample. The mass distribution of the resulting sample is shown in Fig. 3(a), prior to the application of the invariant mass cut. To estimate the contributions from J/ψ and background candidates, the distribution is fitted by χ^2 minimization to the sum of a double-Gaussian function and a linear term, within the range $2.8 < M(\mu\mu) < 3.4 \text{ GeV}/c^2$. From this

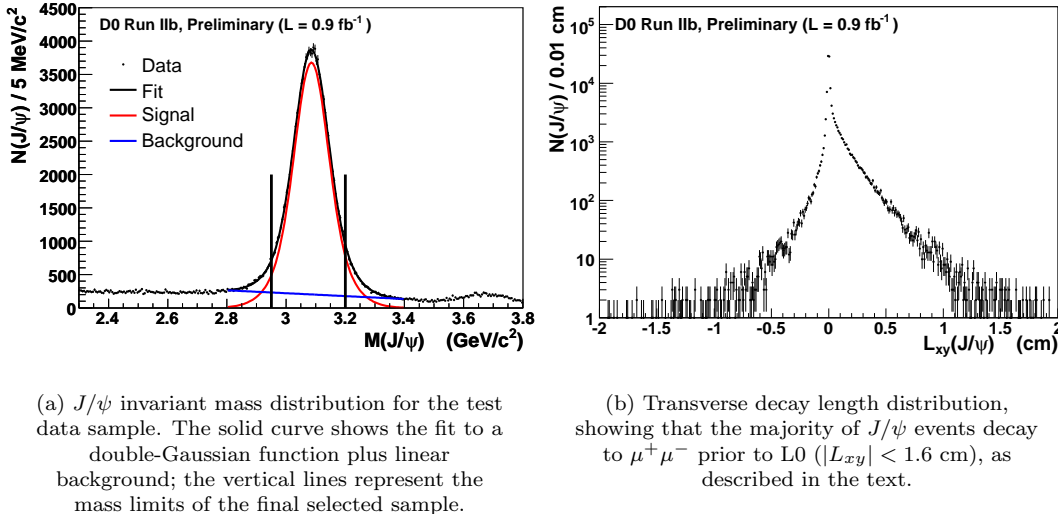


FIG. 3: Invariant mass distribution (a) and transverse decay length (b) of the $J/\psi \rightarrow \mu^+\mu^-$ test sample used to determine the dimuon hit efficiency of the L0 silicon detector.

fit, the sample composition in the selected mass window is determined to be:

$$N(J/\psi) = 109\,249 \pm 698, \quad (2)$$

$$N(\text{bckg}) = 9\,914 \pm 288, \quad (3)$$

$$N(\text{total}) = 119\,163 \pm 755. \quad (4)$$

The result of this fit is consistent with the observed number of events in the sample, 119276. The fit returns a χ^2 of 81, with 113 degrees of freedom. Note that this is before any loose or tight selections are made.

Since the test sample is used to measure the relative tight/loose efficiency for dimuon events, all dimuon production vertices must lie within L0, i.e. less than 1.6 cm from the detector z -axis. This is tested by examining the transverse decay length L_{xy} of the J/ψ events, defined as the distance in the transverse plane between the primary interaction vertex and the J/ψ decay vertex. The distribution of this variable for the entire test sample is shown in Fig. 3(b). J/ψ events are mainly produced promptly, or from B hadron decays, i.e. $B \rightarrow J/\psi X$. The finite lifetime of the B mesons can clearly be seen in the positive values of L_{xy} . More than 99.89% of the dimuons have $|L_{xy}| < 1.6$ cm, and the outlying candidates are excluded from the sample by explicitly enforcing this requirement. Negative decay lengths occur when the particle is reconstructed as travelling towards the primary vertex; this can happen in cases where the spatial resolution of the decay vertex is comparable to the decay length, i.e. the prompt J/ψ and $B \rightarrow J/\psi X$ distributions at short decay lengths are smeared by the effect of the vertex reconstruction resolution.

b. Measuring the Tight/Loose Efficiency

Having defined a test sample of 119276 events, consisting largely of dimuons from $J/\psi \rightarrow \mu^+\mu^-$ decay, with reconstructed origins within the L0 detector, we now proceed to measure the tight selection efficiency for muons, relative to the loose selection. This efficiency can depend on the kinematic and geometrical properties of both muons. To account for these single-muon properties, the efficiency is calculated on a per-muon basis, with the combined dimuon event efficiency given by the product of the efficiencies for the constituent muons:

$$\varepsilon_{T/L} = \varepsilon_{T/L}(\mu_1) \cdot \varepsilon_{T/L}(\mu_2), \quad (5)$$

where $\varepsilon_{T/L}(\mu_i)$ is the relative tight/loose efficiency for a single muon, and is a function of the muon properties described above. The remainder of this section investigates such dependencies, to arrive at a description of the tight/loose efficiency. This will then be used in Section 7 to calculate the number of dimuon candidates in which one or more muons are produced outside L0. For convenience, the notions of tight and loose selections are extended to cover the single muon case: a loose muon must have three or more SMT hits, while a tight muon must

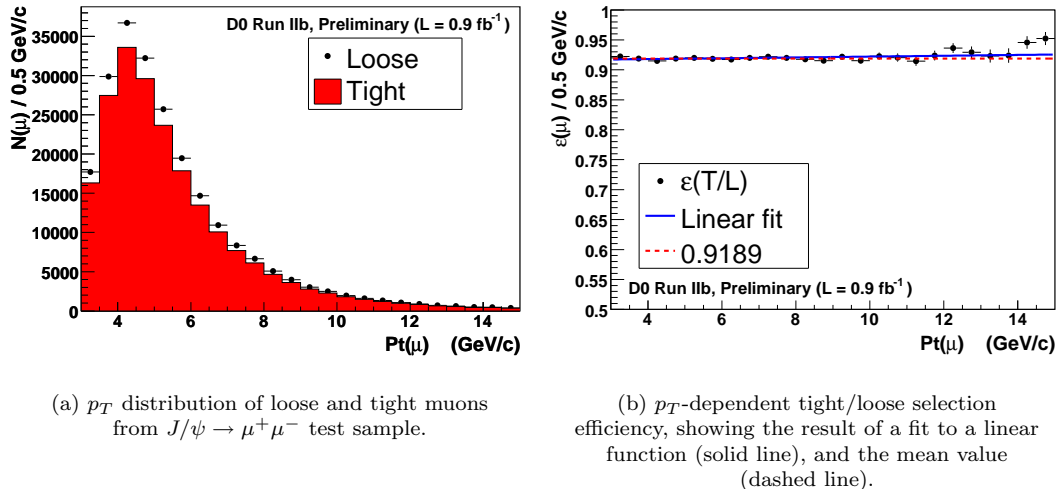


FIG. 4: The relative tight/loose selection efficiency for individual muon candidates, as a function of their transverse momentum.

also be associated with a hit in the L0 detector. A loose (tight) *event* is one in which both muons are loose (tight). The mean single-muon efficiency is first calculated, starting with the $119\,276 \times 2 = 238\,552$ muons in the full signal sample.

$$\begin{aligned}
 N_{\mu}(\text{loose}) &= 228\,569, \\
 N_{\mu}(\text{tight}) &= 210\,026, \\
 \varepsilon_{T/L}(\mu) &= 0.9189 \pm 0.0006, \\
 \varepsilon_{T/L} &= 0.8443 \pm 0.0008.
 \end{aligned} \tag{6}$$

Here the uncertainty is purely statistical, and is determined using the standard binomial expression $\sigma[\varepsilon_{T/L}(\mu)] = \sqrt{\varepsilon_{T/L}(\mu)[1 - \varepsilon_{T/L}(\mu)]/N_{\mu}(\text{loose})}$.

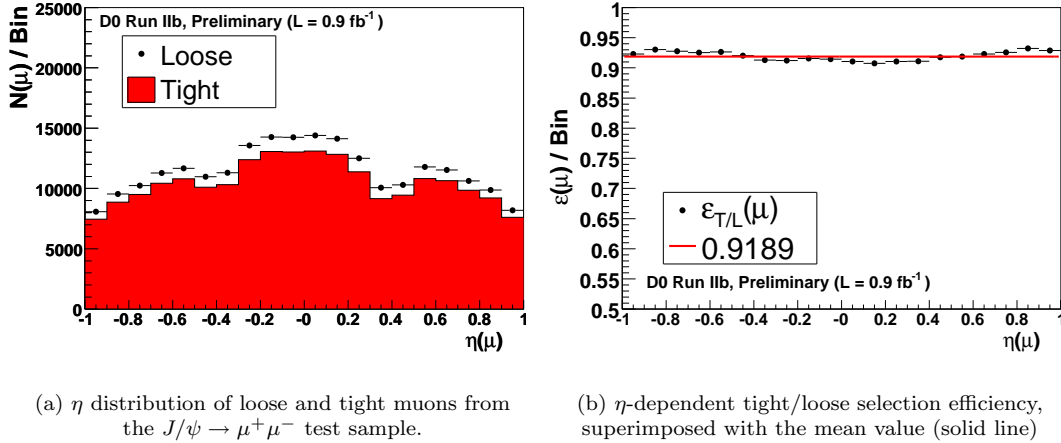
Figure 4(a) shows the transverse momentum distributions for loose and tight muons. The efficiency is then calculated for each p_T bin by dividing the histograms, as shown in Fig. 4(b). Here and in other efficiency distributions, the uncertainty on each entry is calculated using the appropriate binomial relation. There is some indication that higher- p_T muons have higher L0 efficiencies, at the $\sim 1\%$ level, which is quantified by fitting the resulting distribution to a first degree polynomial, yielding the following parameterization:

$$\begin{aligned}
 \varepsilon(p_T) &= a + b \cdot (p_T - 9), \\
 a &= 0.9214 \pm 0.0011, \\
 b &= 0.0007 \pm 0.0003,
 \end{aligned} \tag{7}$$

where the transverse momentum is in units of GeV/c . The fit gives a minimum χ^2 of 31, with 22 degrees of freedom. The transverse momentum dependence is a very small effect, accounting for an increase in efficiency of only 1% over the full p_T range, and around half of that variation in the dominant region $p_T < 8 \text{ GeV}/c$. The apparent dependence could be caused by other effects, such as correlations with the muon pseudorapidity. Therefore, we repeat the event counting procedure with no p_T dependence in the efficiency model, and assign a systematic uncertainty given by the resulting shift in the determined number of excess events.

A similar calculation is carried out for the muon pseudorapidity η . The distribution for loose and tight muons from J/ψ events is shown in Fig. 5(a), with the resulting efficiency distribution shown in Fig. 5(b). Unlike the p_T case, there are significant changes in efficiency across the selected pseudorapidity range; the fluctuations are still small with respect to the efficiency, with the maximum and minimum values differing by $< 3\%$. This variation is taken into account when determining the efficiency, on a bin-by-bin basis, as described later in this section.

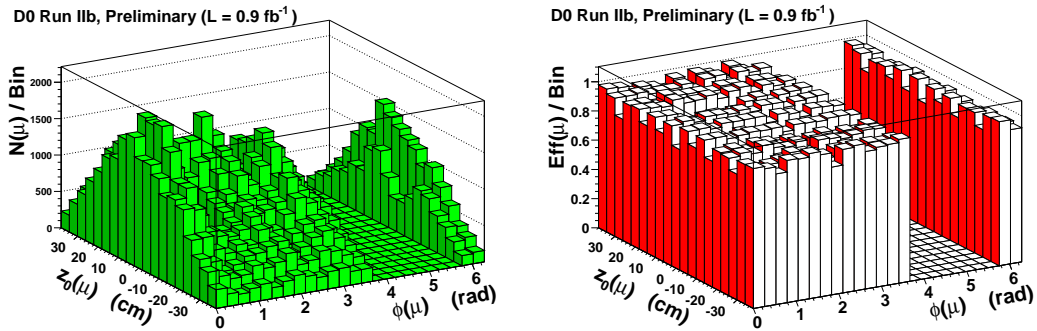
Since the L0 detector is constructed from forty-eight sensors arranged in (z, ϕ) segments, it is important to characterize the efficiency as a function of these two variables. In this way the effects of varying sensor performance are accounted for in the subsequent studies of the signal dimuon sample. Figure 6 shows the two-dimensional (z, ϕ) distribution of muons from tight and loose events, with twenty-four bins in ϕ , and nineteen in z . Here the coordinates are



(a) η distribution of loose and tight muons from the $J/\psi \rightarrow \mu^+\mu^-$ test sample.

(b) η -dependent tight/loose selection efficiency, superimposed with the mean value (solid line)

FIG. 5: The relative tight/loose detection efficiency for muons from J/ψ decays, as a function of their pseudorapidity η . The dips in acceptance at $\eta = \pm 0.4$ in (a) are due to the arrangement of detection elements in the muon system.



(a) (z, ϕ) distribution of loose muons from the J/ψ test sample. The z -dependence is due to the beam-crossing dynamics.

(b) Two-dimensional (z, ϕ) -dependent tight/loose selection efficiency. The low bins in z are associated with the ~ 1 mm gaps between the sensors.

FIG. 6: The L0 detection efficiency for muon candidates, as a function of their azimuthal angle (ϕ) and z -coordinate of the muons at their point-of-closest-approach to the L0 detector. Departures from the mean efficiency are a consequence of the geometrical segmentation of the detector sensors, each of which can have a different efficiency.

measured at the point-of-intersection with the appropriate L0 sensor. Note that events with muons passing through regions with poor acceptance have already been explicitly removed. The corresponding efficiency distribution is shown in Fig. 6(b). Variations in efficiency are visible, and must be accounted for in subsequent calculations.

The relative efficiency of loose and tight requirements for dimuon events can now be determined as a function of the pseudorapidities, transverse momenta, and (z, ϕ) coordinates of the muon pair (μ_1, μ_2) . The total efficiency is taken as the product of the efficiencies for the individual muons, as in Eq. (5), where the individual muon efficiency is considered as the product of kinematic and geometrical contributions:

$$\varepsilon(\mu_i) = \varepsilon(z_{\mu_i}, \phi_{\mu_i}) \cdot \mathcal{F}(\eta_{\mu_i}) \cdot \mathcal{F}(p_T^{\mu_i}). \quad (8)$$

The geometrical efficiency $\varepsilon(z_{\mu_i}, \phi_{\mu_i})$ is taken directly from the histogram shown in Fig. 6(b). The additional factors are modeled as follows. The normalized transverse momentum dependence is parameterized as:

$$\mathcal{F}(p_T^{\mu_i}) = \frac{a + b \cdot (p_T^{\mu_i} - 9)}{a}, \quad (9)$$

with a and b fixed according to Eq. (7), and transverse momentum in units of GeV/ c . The denominator in this

expression is required in order to normalize the effect of this additional correction; for muons with transverse momenta larger than 15 GeV/ c , the p_T correction is fixed to unity. The normalized pseudorapidity dependence $\mathcal{F}(\eta_{\mu_i})$ is taken directly from the histogram H in Fig. 5(b), with each muon attributed a factor:

$$\mathcal{F}(\eta_{\mu_i}) = H(\eta_{\mu_i})/0.9189, \quad (10)$$

where the denominator again ensures that the η -averaged effect of this correction is normalized to unity.

Statistical uncertainties associated with the efficiency measurement are propagated through all calculations. The uncertainty on the geometrical efficiency for each bin is determined using the standard binomial expression; the same procedure is also carried out for the η factor, while the uncertainties on the transverse momentum model can be taken from the one standard deviation limits on a and b determined by the χ^2 minimization. The uncertainty propagation is described in more detail in the next section, and the estimation of systematic uncertainties is described in Section 8.

7. RESULTS

a. Determining $N(\text{excess})$

The number of loose and tight dimuons in the signal sample can now be used, in conjunction with the efficiency determination from the previous section, to estimate the number of events in which one or both of the muons are produced beyond L0. In total, the signal sample contains 204 177 dimuon events, of which 177 535 satisfy the loose silicon hit requirements (i.e. three or more hits in the SMT detector). Of these, 149 161 also pass the tight SMT requirement that both muons have a hit in L0. The determination of $N_{\mu\mu}(\text{excess})$ proceeds on an event-by-event basis, using the following relation:

$$N_{\mu\mu}(\text{excess}) = N_{\mu\mu}^{\text{obs}}(\text{loose}) - N_{\mu\mu}^{\text{exp}}(\text{loose}). \quad (11)$$

Here $N_{\mu\mu}^{\text{obs}}(\text{loose})$ is the observed number of events in the loose sample; $N_{\mu\mu}^{\text{exp}}(\text{loose})$ is the number of expected events, calculated by applying the efficiency as follows:

$$N_{\mu\mu}^{\text{exp}}(\text{loose}) = \sum_{i=1}^{N_{\mu\mu}(\text{tight})} \frac{1}{\varepsilon_{T/L}^i} \equiv \frac{N_{\mu\mu}(\text{tight})}{\langle \varepsilon_{T/L} \rangle}, \quad (12)$$

where the summation is over all tight events, and the efficiency for an event is given by Eqs. (5,8–10). Here the equation has been rearranged in terms of an effective mean efficiency $\langle \varepsilon_{T/L} \rangle$ to return the format of Eq. (1). Throughout the following discussion, all numbers represent dimuon event counts, and the $\mu\mu$ subscript is dropped for clarity.

This calculation is performed separately for opposite-sign (OS) and same-sign (SS) dimuon events. The full results are shown in Table I, and the number of events with one or both muons produced outside L0 is found to be:

$$N(\text{excess}) = 712 \pm 462 \pm 942 \quad (\text{Total}), \quad (13)$$

$$= 2 \pm 359 \pm 705 \quad (\text{Opposite-sign dimuons}), \quad (14)$$

$$= 710 \pm 138 \pm 229 \quad (\text{Same-sign dimuons}), \quad (15)$$

where the first uncertainty is statistical, and the second systematic (described below). The contributions from same-sign and opposite-sign muons are therefore consistent within uncertainties. This excess can also be expressed as a fraction of the total loose sample:

$$N(\text{excess})/N^{\text{obs}}(\text{loose}) = (0.40 \pm 0.26 \pm 0.53) \%. \quad (16)$$

The uncertainty $\sigma[N(\text{excess})]$ is evaluated as follows. Equation (11) is first rearranged to define $N(\text{excess})$ in terms of the independent variables $N(\text{tight})$ and $N(L\bar{T}) = [N^{\text{obs}}(\text{loose}) - N(\text{tight})]$:

$$N(\text{excess}) = N(L\bar{T}) - N(\text{tight}) \cdot \frac{1 - \langle \varepsilon_{T/L} \rangle}{\langle \varepsilon_{T/L} \rangle}. \quad (17)$$

The total uncertainty is then given by appropriate combination in quadrature of the uncertainties on $N(L\bar{T})$, $N(\text{tight})$ and $\langle \varepsilon_{T/L} \rangle$. The determination of systematic uncertainties is described in Section 8. The statistical uncertainty on the number of events is simply the square root of the number. For the effective mean efficiency the statistical uncertainty

TABLE I: Event counts for signal dimuon events. The number of loose, $N^{\text{obs}}(\text{loose})$, and tight, $N(\text{tight})$, events are taken from data. The contribution to the loose sample from production inside L0, $N^{\text{exp}}(\text{loose})$, is determined using Eq. (12). The method for evaluating the uncertainty σ on each of these quantities is described in the text.

	Total	Opposite-sign	Same-sign
$N(\text{tight})$	149 161	113 088	36 073
$N^{\text{obs}}(\text{loose})$	$177\,535 \pm 421$	$134\,097 \pm 437$	$43\,438 \pm 208$
$N^{\text{exp}}(\text{loose})$	$176\,823 \pm 503$	$134\,095 \pm 382$	$42\,728 \pm 121$
$N(\text{excess})$	712 ± 462	2 ± 359	710 ± 138

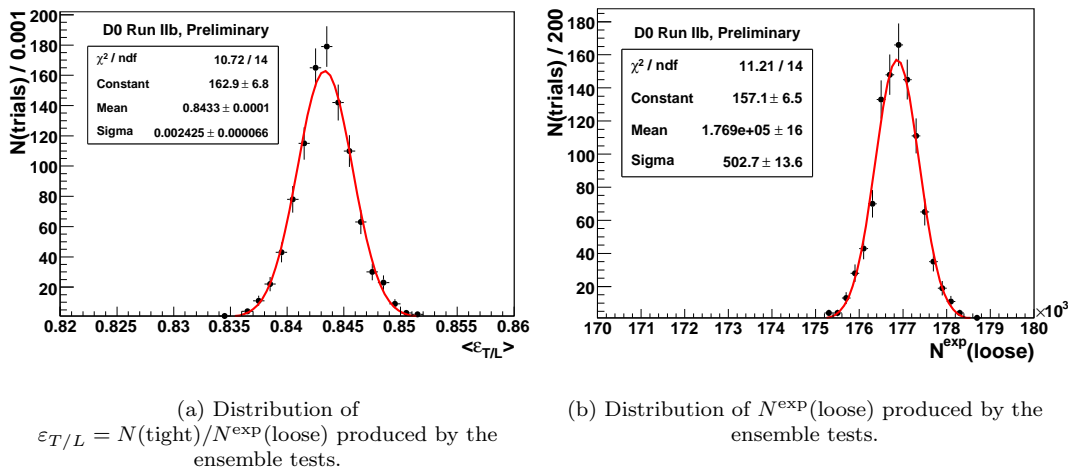


FIG. 7: Results of the ensemble test for dimuons of all sign-combinations. The markers show the distribution of $\varepsilon_{T/L}$ and $N^{\text{exp}}(\text{loose})$, as determined by each of the 1000 trials. The solid lines show the results of fitting to Gaussian functions.

is determined using ensemble tests, in which the calculation of Eq. (11) is repeated 1000 times, with the constituent efficiency factors allowed to vary in a well-defined manner, as described below.

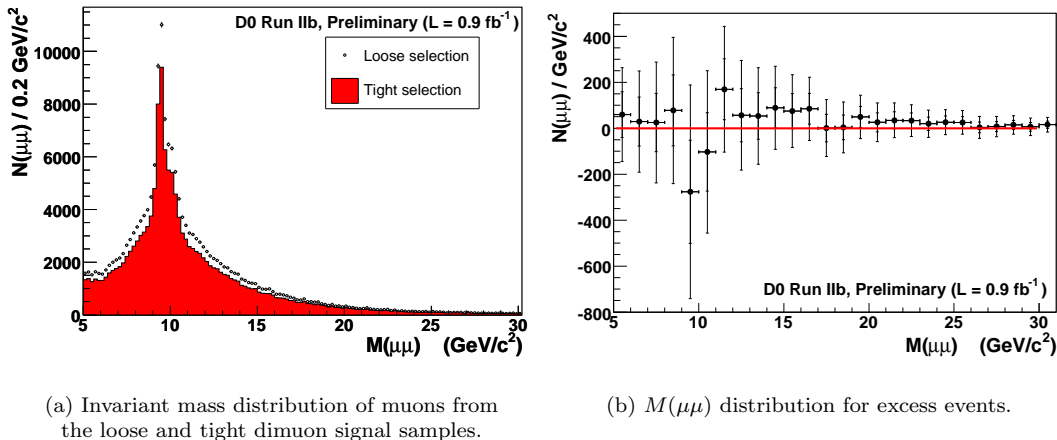
The efficiency in each (ϕ, z) bin, the efficiency in each η bin, and the parameters a and b in the transverse momentum factor, are all assigned pseudo-randomly according to a Gaussian distribution, with an appropriate mean and standard deviation. The distribution of $\langle \varepsilon_{T/L} \rangle$, as returned by each separate run, is then fitted to a Gaussian function to extract the uncertainty on this quantity. Figure 7(a) shows the result of this operation for the total sample, with no sign requirements on the dimuon candidate: the efficiency is well-parameterized by this function with width $\sigma = 0.0024$. The associated distribution of $N^{\text{exp}}(\text{loose})$ is shown in Fig. 7(b), also fitted to a Gaussian function.

b. Normalising $N(\text{excess})$ to the J/ψ Signal

As a point of normalization for the selected signal dimuon loose sample, we give the number of events in the J/ψ mass peak, when the lower mass limit of $5 \text{ GeV}/c^2$ is removed. This peak will have many events in common with the J/ψ test sample, but will not be exactly the same due to the additional vertex constraints used in isolating the test candidates. The resulting mass peak contains $165\,489 \pm 969$ in total, determined from a χ^2 minimization fit using the same parameterization as described in Section 6 a. Therefore, the number of excess events observed in the mass range $(5 < M(\mu\mu) < 80) \text{ GeV}/c^2$ is a fraction $(0.43 \pm 0.28 \pm 0.57)\%$ of the number of J/ψ candidates under identical selection requirements (except for the removal of the minimum invariant mass criterion).

c. Distributions of $N(\text{excess})$

In addition to determining the total number of excess events, it is informative to count the number of excess events separately in sub-regions of various kinematic or angular parameters, to look for possible enhancements of



(a) Invariant mass distribution of muons from the loose and tight dimuon signal samples.

(b) $M(\mu\mu)$ distribution for excess events.

FIG. 8: Invariant mass distributions for signal dimuons. The background-subtraction method described in the text is used to extract the distribution for excess events (b), which can be compared to the distribution for loose and tight events shown in (a). For each point, the smaller error bar represents the statistical uncertainty, and the larger error bar also includes the effect of systematic uncertainties on the efficiency. The uncertainties are correlated between bins, since they include contributions from $\sigma(\epsilon_{T/L})$.

excess dimuon events. This is equivalent to producing the distribution of excess events for different variables: the event-by-event efficiency allows such distributions to be obtained. The expected distribution for loose events is first produced by repeating the calculation in Eq. (12) separately for each bin in the tight histogram. The distribution of excess events can then be determined by subtracting this expectation from the observed loose event histogram, i.e. by applying Eq. (11) on a bin-by-bin basis.

Figure 8 shows the number of excess events versus the dimuon invariant mass. The distributions for loose and tight events are shown in Fig. 8(a); After subtracting $N^{\text{exp}}(\text{loose})$ from the observed loose distribution, the distribution of $N(\text{excess})$ is produced as shown in Fig. 8(b). The lack of an Υ resonance in the excess sample is an indication that the expectation-subtraction procedure is correctly accounting for contributions from prompt muon sources. In this and other excess distributions, the smaller error bar represents the statistical uncertainty, and the larger error bar also includes the effect of systematic uncertainties. These uncertainties are correlated between bins, since they include contributions from the efficiency, as quantified in Eq.(17).

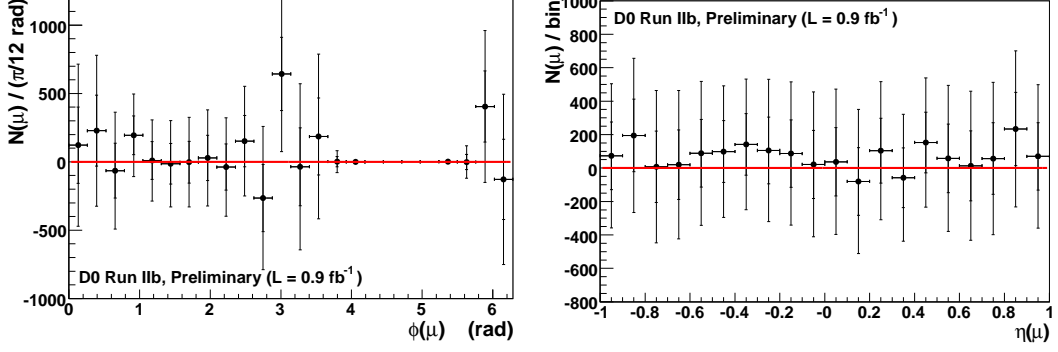
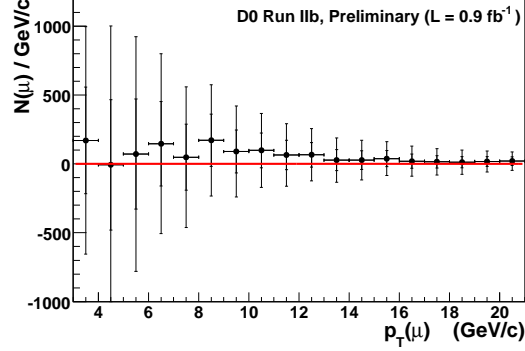
The same procedure can be repeated for other variables of interest. Figure 9 shows the distribution of the azimuthal angle, pseudorapidity, and transverse momentum of the individual muons. The excess muons show no significant dependence on any of these kinematic or angular variables.

The impact parameter distributions for muons from loose and tight events are shown in Fig. 10. Producing the corresponding distribution for muons from excess events is complicated. This is because the shape is strongly affected by the different impact parameter resolutions for tracks with and without L0 hits [6]. Since this effect is dependent on the track orientation and transverse momentum, the current analysis makes no attempt to correct for this effect, and the excess IP distribution is not presented.

8. SYSTEMATIC UNCERTAINTIES AND CONSISTENCY CHECKS

Various sources of systematic uncertainty on the event counting procedure are considered, and their effects quantified. The summary of these contributions to $N(\text{excess})$ is shown in Table II. The calculation of efficiency was repeated with different binning schemes for the ϕ , z , and η histograms. In addition, the p_T factor is removed from the efficiency parameterization. The maximal difference in the fraction $N(\text{excess})/N(\text{loose})$ under these modified counts is translated into an uncertainty on $N(\text{excess})$.

To check that the inclusive trigger selection does not bias the number of excess events in the sample, the study is repeated using only those events which are selected by the non-track-matched dimuon trigger described in Section 3. The conclusions are consistent with the inclusive trigger selection, with $N(\text{excess})$ comprising a fraction 0.32% of the loose sample (396 / 123,572). In addition, the sample is divided into two time eras corresponding to the data collection date, and consistent results are observed within statistical fluctuations, with $N(\text{excess})/N^{\text{obs}}(\text{loose})$ measured to be

(a) ϕ distribution for excess events.(b) η distribution for excess events.

(c) Transverse momentum distribution for excess events.

FIG. 9: Azimuthal angle, pseudorapidity, and transverse momentum distributions for excess muons from the signal dimuon sample. For each point, the smaller error bar represents the statistical uncertainty, and the larger error bar also includes the effect of systematic uncertainties on the efficiency. The uncertainties are correlated from bin-to-bin, since they include contributions from $\sigma(\varepsilon_{T/L})$.

TABLE II: Systematic uncertainties on $N(\text{excess})$, determined using the methods described in the text.

Source	$\delta[\%(\text{excess})]$
Rebin ϕ	$\pm 0.14\%$
Rebin z	$\pm 0.18\%$
Rebin η	$\pm 0.01\%$
$\mathcal{F}(p_T^\mu)$ Removed	$\pm 0.48\%$
Total	$\pm 0.53\%$

0.48% and 0.25% for the two samples.

The two-dimensional scatter plots of $\text{IP}(\mu_1)$ vs. $\text{IP}(\mu_2)$, for both loose and tight signal selections, are shown in Fig. 11. The absence of events on the leading diagonal indicates the very small contribution from through-going cosmic ray muons. Most events are associated with one or both muons having very small impact parameter, as expected. All tight dimuons are contained in the region ($|\text{IP}_{\mu_1}| < 1.6$ cm, $|\text{IP}_{\mu_2}| < 1.6$ cm), as expected, whereas loose events are observed with impact parameters up to 2.5 cm.

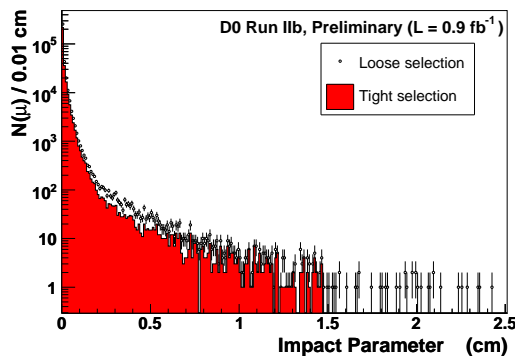
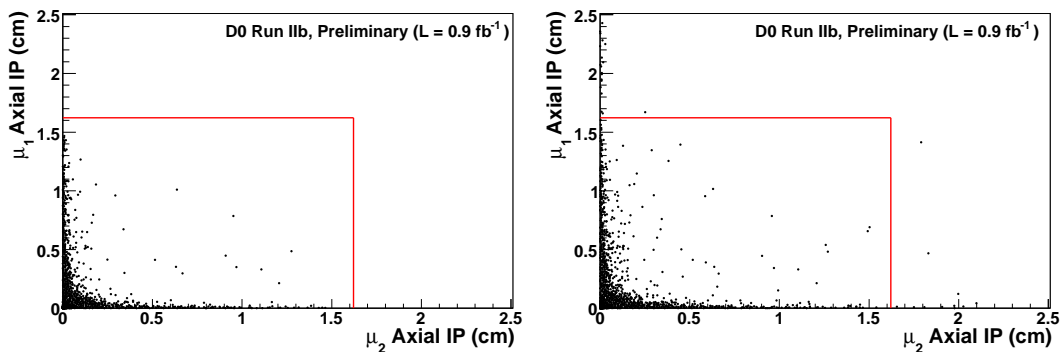


FIG. 10: Impact parameter distributions for muons from the loose and tight signal dimuon samples. Muons from tight events exhibit a sharp cut-off at $IP < 1.5$ cm, while the loose sample contains muons with impact parameters up to 2.5 cm.



(a) Tight selection.

(b) Loose selection.

FIG. 11: Two-dimensional impact parameter distribution of all signal events in the tight and loose dimuon sample, with the inner radius of the L0 detector shown by the solid lines. The lack of events on the leading diagonal indicates that contamination from cosmic ray muons is minimal. Very few events are observed in which both impact parameters are large.

9. POSSIBLE SOURCES OF EXCESS EVENTS

Although the nominal excess is not significant, we have considered a number of sources which produce reconstructed muons originating beyond the beampipe region, including hadronic punch-through, pion and kaon decay-in-flight, and cosmic ray muons. As the muons are required to exit the iron toroid, which is over 13λ thick (at $\eta = 0$), hadronic punch-throughs are negligible in this analysis [13, 14]. In addition, punch-throughs come directly from the primary vertex and would therefore be accounted for by the efficiency-weighted extrapolation process.

a. Decays in Flight

Pion and kaon decays in flight, i.e. $\pi \rightarrow \mu\nu$ and $K \rightarrow \mu\nu$, lead to muon production outside the beampipe region. Charged π/K mesons which decay in the central tracking detector will have the initial portion of their trajectory coming from the primary vertex. However, the fitting procedure does not include the kink at the decay point and so fit outputs such as momentum, the quality of the fit, and the impact parameter will be degraded, with this effect being larger for kaons. For the impact parameter, this degradation will be worse if the decay occurs earlier in the flight path. For a momentum of 10 GeV/c, about 0.06% of charged pions and 0.5% of charged kaons will decay in the first 35 cm, although there are many more pions than kaons in a typical event. For decays in flight with kinks inside the beampipe or SMT, only the muon beyond the kink is reconstructed as a track, resulting in large reconstructed impact parameters. Decay-in-flight muons originating inside the beampipe will almost always enter the tight dimuon sample, as a result of the high efficiency of L0. As such there will be contributions from this source to both the loose

and tight samples.

A previous D0 analysis of CP-violating parameters in dimuon charged asymmetry found that about 5% of events had a prompt muon plus a K^\pm decay [15]. This analysis required $p_T(\mu) > 4.2$ GeV/ c and impact parameter < 0.3 cm, and additional studies will be performed to estimate this contribution at larger impact parameter.

Another good estimate of the contribution due to decays-in-flight can be found in Ref. [16], where the ratio of candidates in $B^+ \rightarrow J/\psi K^+$ and $B^+ \rightarrow J/\psi \mu^+$ mass peaks is examined. The results show that a fraction $(3.4 \pm 0.2)\%$ of these candidates have a $K \rightarrow \mu\nu$ decay in flight.

Neutral kaons can also produce muons with naturally large displacements from the primary vertex. The decay probability for K_S and K_L with $p = 10$ GeV/ c in the first 35 cm are about 50% and 0.2% respectively. Around 27% of K_L decays result in muons, via the process $K_L \rightarrow \pi\mu\nu$. For K_S mesons, muons arise for around 1% of decays, via the secondary pion decay $K_S \rightarrow \pi\pi$, $\pi \rightarrow \mu\nu$. Each neutral weak eigenstate yields muons at approximately 10% of the K^\pm rate, but with a different and more extended impact parameter distribution. Events which have both muons coming from π or K decay are dominated by multi-jet events without heavy quarks. The ratio of these to dimuons from b and c is less than 1%.

b. Cosmic Ray Muons

Another expected source of muons with large displacements from the primary vertex are cosmic ray muons. There are three distinct topologies. A single muon can enter and exit the detector and so have its two reconstructed tracks be back-to-back. One can also have cosmic ray showers with multiple muons in time with each other but not back-to-back. The third source is cosmic ray muons coinciding with a beam-produced muon, which have a greater likelihood to be close to vertical but are otherwise uncorrelated with the prompt muon. The first two sources can produce correlated tracks originating outside the beampipe. In each case the time distribution in the muon system scintillation counters can be shifted relative to prompt muons and the time difference between the scintillator outside and inside the iron is shifted by about 20 ns for entering cosmic ray muons. Studies of the scintillation counter timing, using variables such as $t_A(\mu_1) - t_C(\mu_1)$, and $t_C(\mu_1) - t_C(\mu_2)$ allow estimates of the contribution of cosmic to be made. Using these methods, it is estimated that the total contribution to the excess sample from cosmic ray muons is less than 100 events (95% C.L.), corresponding to a fraction 0.06% of the loose sample.

10. CONCLUSIONS

Using 0.9 fb^{-1} of integrated luminosity, a sample of dimuon events is examined with similar event characteristics as those selected in the CDF multi-muon analysis [1]. We measure the fractional excess of muons produced in the silicon detector outside of the beampipe to be $(0.40 \pm 0.26 \pm 0.53)\%$, significantly smaller than the $\sim 12\%$ observed by CDF [1]. The D0 excess is expected to have contributions from mainly K and π decays in flight, as well as residual cosmic ray contamination, and further studies are in progress to quantify the composition. Examination of the properties of this excess indicate that these events are not enhanced in any particular kinematic regions in η , ϕ , p_T or $M(\mu\mu)$.

Acknowledgements

We thank the staffs at Fermilab and collaborating institutions, and acknowledge support from the DOE and NSF (USA); CEA and CNRS/IN2P3 (France); FASI, Rosatom and RFBR (Russia); CNPq, FAPERJ, FAPESP and FUNDUNESP (Brazil); DAE and DST (India); Colciencias (Colombia); CONACyT (Mexico); KRF and KOSEF (Korea); CONICET and UBACyT (Argentina); FOM (The Netherlands); STFC (United Kingdom); MSMT and GACR (Czech Republic); CRC Program, CFI, NSERC and WestGrid Project (Canada); BMBF and DFG (Germany); SFI (Ireland); The Swedish Research Council (Sweden); CAS and CNSF (China); and the Alexander von Humboldt Foundation (Germany).

-
- [1] T. Aaltonen *et al.* [CDF Collaboration], arXiv:0810.5357 [hep-ex].
 - [2] B. Abbott *et al.* [D0 Collaboration], Phys. Rev. Lett. **84**, 5478 (2000).
 - [3] P. Nason, arXiv:hep-ph/0301003.
 - [4] M. L. Mangano, AIP Conf. Proc. **753**, 247 (2005).
 - [5] V. M. Abazov *et al.* [D0 Collaboration], Nucl. Instrum. Meth. A **565**, 463 (2006).
 - [6] D. Tsybychev [D0 Collaboration], Nucl. Instrum. Meth. A **582**, 701 (2007).
 - [7] V. M. Abazov *et al.*, Nucl. Instrum. Meth. A **552**, 372 (2005).

- [8] J. Abdallah *et al.* [DELPHI Collaboration], *Eur. Phys. J. C* **32**, 185 (2004).
- [9] V. M. Abazov *et al.* [D0 Collaboration], *Phys. Rev. Lett.* **97**, 161802 (2006).
- [10] V. M. Abazov *et al.* [D0 Collaboration], D0 Note 5023-CONF, (2006).
- [11] C. Amsler *et al.*, *Physics Letters B* **667**, 1 (2008).
- [12] J. Abdallah *et al.* [DELPHI Collaboration], *Astropart. Phys.* **28**, 273 (2007).
- [13] D. Green and D. Hedin, *Nucl. Instrum. Meth. A* **297**, 111 (1990).
- [14] D. Green *et al.*, *Nucl. Instrum. Meth. A* **244**, 356 (1986).
- [15] V. M. Abazov *et al.* [D0 Collaboration], *Phys. Rev. D* **74**, 092001 (2006).
- [16] V. M. Abazov *et al.* [D0 Collaboration], *Phys. Rev. Lett.* **102**, 092001 (2009).